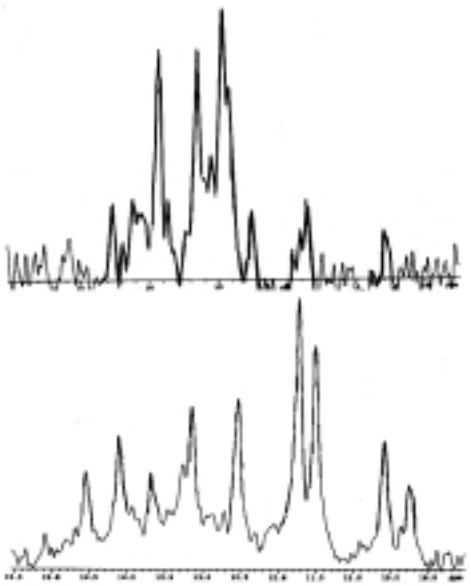

been carried out on solutions containing approximately 1 mM RNA. Analysis of TOCSY spectra of aromatic protons of the uncapped molecule has verified that the folded SL adopts a single conformation. The pattern of imino proton resonances in spectra of exchangeable protons reveals both Watson-Crick and non-Watson-Crick base pairing and suggest a complex fold for the RNA. Imino proton resonances of the capped RNA were substantially altered in location and relative intensity. We conclude that the presence of a 5' cap induces a markedly different folded structure. In collaboration with Prof. Martin Schwartz's laboratory (Dept. of Chemistry, FSU), we have begun synthesis of a trimethylguanosine capped spliced leader that will be used for further structure determination.

**Figure 1.** Imino proton regions of exchangeable 1H spectra performed at 1 °C. Top spectrum is capped RNA. Bottom spectrum is uncapped RNA.



# GEOCHEMISTRY

## Analysis of Organic Phosphorus in Surface Waters from the Florida Everglades by Capillary Electrophoresis and High Performance Liquid Chromatography Coupled to Inductively Coupled Plasma Mass Spectrometry

Bennett, L., NHMFL/FSU, Geological Sciences
Salters, V.J.M., NHMFL/FSU, Geological Sciences
Cooper, W., NHMFL/FSU, Geological Sciences

Nutrient loading has become a significant problem in many ecosystems, and especially in the Florida Everglades. Increases in phosphorus (P) have been linked to many alterations in this naturally oligotrophic ecosystem, including taxonomic shifts and eutrophication. A concerted effort to reduce phosphorus entering the Everglades was begun with the construction of the Everglades Nutrient Removal Project (ENR), the largest treatment wetland in North America. Verification of the efficacy of the ENR requires the development and application of specialized analytical techniques that can determine various organic-P species at environmentally significant levels.

Inductively coupled plasma mass spectrometry (ICP-MS) is a sensitive and selective technique for determining low levels (~1 ppb) of P in liquid matrices. Last year we demonstrated that ICP-MS analysis of Everglades water samples was superior to conventional colorimetric methods for total P analysis at both low P concentrations and at high organic carbon content.

This year we have coupled Capillary Electrophoresis (CE) and High Performance Liquid Chromatography (HPLC) with element-specific ICP-MS detection in order to quantitate individual types of organic phosphorus compounds in the Florida Everglades. Both are high resolution, physical separation methods that can isolate individual classes of organo-phosphates before P-specific detection. CE separates individual species in a microcolumn across which a high electric field is maintained. Separations are based on differences in charge and mass of the analytes. Owing to the complexity of natural water samples, many compounds have similar charge to mass ratios, and thus CE electropherograms obtained with non-specific detectors are broad distributions with little if any resolution of individual compounds. However, the separation of all compounds in a complex sample is not necessary when ICP-MS element-specific detection is employed, but rather only the separation of individual phosphorus species.

Interfacing a Capillary Electropherograph to the ICP-MS was accomplished by connecting the column to a micro-cross with a make-up flow and counter electrode which was inserted into a standard micro-flow nebulizer and spray chamber of the ICP source. An electropherogram of Everglades water is shown in Figure 1. The numerous discrete peaks in this electropherogram demonstrate the presence of several individual organo-phosphates.

HPLC is a column separation technique based on the distribution of solutes between mobile and stationary phases. The principal advantage of HPLC over CE is that fractions coming off the chromatography column can be collected and subjected to further analyses. When operated in the ion-pair mode (HPIPC), charged analytes can be separated in a pseudo ion-exchange manner. Again, by using the ICP-MS as a P-specific

detector, only separation of individual organic-P species need be accomplished.

Everglades water samples were by analyzed by HPIPC, fractions collected in 1mL increments and the fractions analyzed individually for P content. The stacked "phosphograms" of four Everglades samples analyzed in this way with off-line ICP-MS detection are shown in Figure 2. Figure 2 demonstrates the ability of HPIPC with ICP-MS detection to distinguish between various organic-P species. Our results indicate that organic phosphorus compounds leaving the ENR are smaller and probably more bioavailable than organic phosphorus in the older, more mature Water Conservation Areas of the Everglades.

Direct interfacing of the LC system to the ICP-MS is now our primary interest. An initial interfacing was accomplished by sampling the LC effluent directly with a micro-flow nebulizer attached to an MCN-6000 (CETAC) membrane desolvator spray chamber. This interface was tested with an ATP standard and the resulting chromatogram is shown in Figure 3.

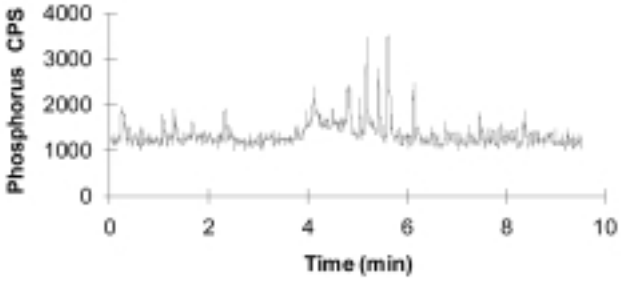


**Figure 1.** "Phosphagram" of P detection for CE-ICP-MS analysis of ENR retentate.

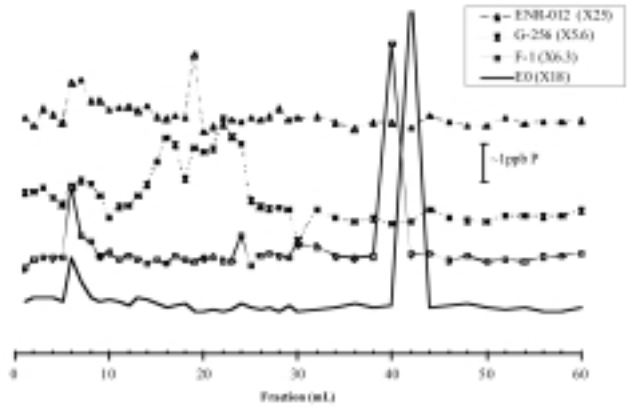


**Figure 2.** IPC separation of 4 Everglades water samples with off-line ICP-MS detection.

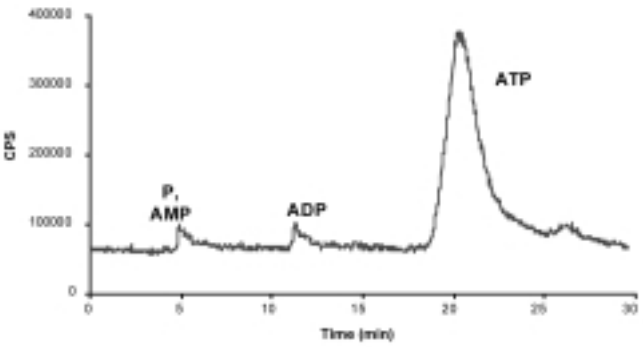


**Figure 3.** Directly coupled HPIPC-ICP-MS analysis of ATP. Conditions: 7.75 mM Tris buffer, pH 7, 3mM TBA, 25% ACN, flow rate 1 mL/min.

## Hf, Nd and Sr Isotope Compositions of Carbonatites

Bizimis, M., NHMFL, Geological Sciences
Salters, V.J.M., NHMFL, Geological Sciences

We report on the Nd, Hf and Sr isotope compositions and trace element concentrations of carbonatite complexes from the East African Rift, South Africa and Canada. On an $\varepsilon_{Nd}$ - $\varepsilon_{Sr}$ diagram the carbonatites from East Africa plot along the East African Carbonatite Line along the lower side of the OIB array. Samples from the Oka carbonatite (Canada) and the Proterozoic S. African complexes all plot within or at the extension of the OIB array within previously defined fields for these complexes.

A characteristic feature of all these carbonatites is their extreme depletions in Hf, Zr, and Ti relative to the adjacent REE and they have high Lu/Hf ratios. Hf isotopes can thus be used to determine whether the high Lu/Hf ratios and by inference the high field strength element (HFSE) depletions are long-lived features of the carbonatite sources or a recent phenomenon.

On a $\varepsilon_{Nd}$ - $\varepsilon_{Hf}$ diagram the E. African carbonatites show a large variation in their Hf isotopic compositions ($\varepsilon_{Hf}$ = -8 to 14) for a limited range in Nd isotopic compositions ($\varepsilon_{Nd}$ = 0 to 4). A sample from Oka complex plots above the OIB array ($\varepsilon_{Hf}$ = 32, $\varepsilon_{Nd}$ = 5) while the S. African carbonatites plot within or above the OIB array. Over 90% of the Hf content of these carbonatites resides in their silicate fraction which consists only 2 to 5% of the whole rock. Hf and Nd isotope data for these silicate fractions show that they are often in isotopic disequilibrium with the whole rocks and may be xenocrystic in origin. Since the Hf whole rock budget is dominated by the Hf content of the silicate fraction then the whole rock Hf isotopic composition may not be representative of the "pure" carbonatite (the carbonate fraction). Mass balance calculations between the whole rocks and silicate fractions suggest that the carbonate phases in some of these carbonatites have highly radiogenic Hf compositions ($\nu_{Hf}$ >40). Nevertheless, the high Lu/Hf ratios (Lu/Hf > 30) in the carbonate phases can develop these very radiogenic Hf

isotopic compositions in a time period comparable with the ages of the carbonatites. Our data suggests that even the carbonatites with the most radiogenic Hf compositions originate from a mantle source that does not have any long term Hf (and by inference Zr and Ti) depletions (see figure). This indiactes that the HFSE depletions in the carbonatites must be related to the melting process and are not a long-lived source characteristic.

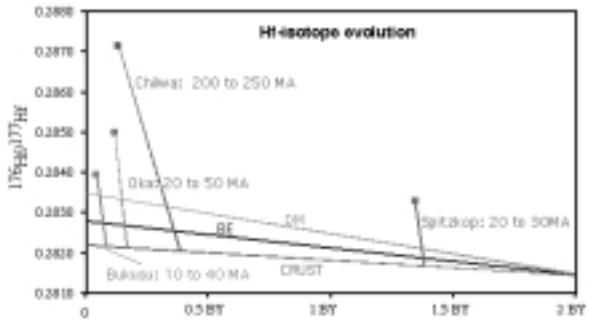


**Figure 1.** The Hf-isotope evolution and model ages for four carbonatites. Evolution lines labeled DM, BE and crust are for depleted mantle, Bulk Earth and continental crust. Evolution lines for carbonatites are very steep reflecting the high Lu/Hf ratio of the materials. Age range indicated with each location name for carbonatites are the range resulting from the intercepts with the different evolution lines. Evolution lines are terminated at the eruption age.

## U-Th Evidence for Crustal Involvement in the Petrogenesis of Nevados de Payachata, Chile

Bourdon, B., Laboratoire de Géochimie et Cosmochemie, IPGP-CNRS
Wörner, G., Universität Göttingen, Geochemistry
Zindler, A., NHMFL/FSU, Geological Sciences

The Nevados de Payachata volcano has erupted through ~70 km of continental crust in the central volcanic zone of the Andes in Chile (18 °S, 69 °W). Recent lavas and mineral separates have been analyzed by mass spectrometry for U-Th disequilibrium, radiogenic isotope ratios, and trace element concentrations. The lavas are characterized both by $^{230}Th$ enrichment and depletion relative to the parent nuclide, $^{238}U$. Minerals separated from individual lavas have been used to derive U-Th isochron ages, and in general, these compare favorably with inferred stratigraphic ages and K-Ar ages.

Despite a relative constancy in Sr, Nd, and Pb isotope ratios, the investigated lavas display inverse trends of $^{230}Th/^{238}U$ versus Ce/Yb or Ba/Hf. These trends cannot be interpreted in terms of simple two-component mixing. Rather, there must be three (and perhaps four) components involved in the genesis of the Parinacota lavas. Namely, source components deriving from the mantle wedge, subducting slab, and the lower continental crust can be identified. A sediment component is more difficult to detect because of the strong crustal influence. The existence of binary arrays can be explained by variable amounts of crustal material.

## Dosimetric Properties of Aluminum Hole Centers in Quartz: Implications for the Nature of Giant Radiation-Induced Color Haloes

Odom, A.L., NHMFL/FSU, Geological Sciences
Xie, J., NHMFL/FSU, Geological Sciences

As part of an ongoing study of the dosimetric properties of trapped hole and electron centers in quartz, samples of pheonocrystic quartz from well dated volcanic rocks have been irradiated to dose levels comparable to those received from the natural background over geologic time. Figure 1 shows the effect of this irradiation on the aluminum hole center population in one typical sample.

Here are shown the relative peak-to-peak intensities of the $[AlO_4]^0$ EPR signals measured in a powder quartz sample that received various doses of γ radiation. $[AlO_4]^0$ center populations grow with increasing dose at the lower levels of radiation. They pass through a maximum and then decrease, in the sample above, apparently, toward a final steady-state concentration of $[AlO_4]^0$ at the higher levels of radiation. The dose level of the maximum intensity, however, is different for other samples quartz. In some the intensities appear to continue to decrease at dose levels approaching a gigrad. The $[AlO_4]^0$ EPR center forms as a hole is trapped at a non-paramagnetic$[AlO_4/M^+]^O$ site (M=H, Li, Na), and the hydrogen or alkali ion diffuse away along the c-axis channel of quartz.[1]

The simulated curve above is based on a model that incorporates both the growth of the centers by hole trapping and the decay of centers due to a competition for holes. Measurements of the $E'_1$ center (a hole trapped at an oxygen vacancy) in irradiated

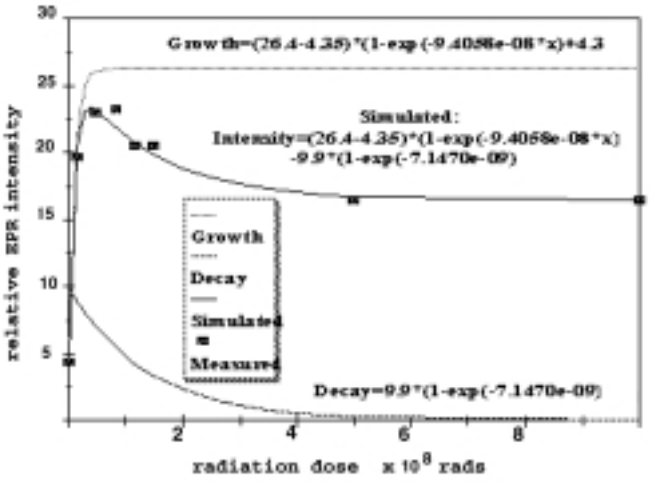


**Figure 1.** Gamma radation dose response of aluminum hole center in alpha quartz.

quartz have shown that new oxygen vacanies are produced at high dose levels.[2,3] In volcanic quartz, substitutional Al sites far outnumber Shottky-Frenkel defects. The initial rapid increase in the $[AlO_4]^0$ population up to the maximum value likely occurs so long as the number of non-paramagnetic $[AlO_4/M^+]^O$ sites is significantly greater than that of oxygen vacancies.

The controversial giant radiation induced color haloes that have been observed surrounding microscopic radioactive inclusions in minerals have most recently been identified in quartz as concentrations of $[AlO_4]^0$ centers, and it was suggested that their sizes are related to hole diffusion and not alpha particle energies.[4] A criticism of this was that it did not explain the absence of observable discoloration inside of the stopping range of known alpha particles. It now seems likely that a lower concentration of Al color centers in the volume of quartz closest to the radioactive inclusions results from the higher radiation dose received there.

1 Halliburton, L.E., Crystal Latt. Defects Amorph. Materials, **12**, 163-190 (1985).
2 Wieser, A. and Regulla, D.F., Rad. Protect. Dosimetry, **34**, 291-294 (1990).
3 Xie, J., Ph. D. dissertation, Florida State University (1998).
4 Odom, A.L. and Rink, W.J., Science, **246**,107-109 (1989).

## Near Kilometer Scale Strontium Isotopic Homogenization in Meta-Granites, North-Central New Mexico

Odom, A.L., NHMFL/FSU, Geological Sciences
Platero, A., San Juan Community College
Sachi-Kocher, A., NHMFL

Strontium within crystalline rocks generally varies in $^{87}Sr/^{86}Sr$ ratio on a scale at least as large as individual mineral crystals. This variation results from different minerals having different ratios of Rb/Sr and the natural β-decay of $^{87}Rb$ to $^{87}Sr$. Such differences in the $^{87}Sr/^{86}Sr$ ratios increase with time, or the age of the rock. There are many well documented examples of isotopic homogenization occurring during metamorphism, when temperatures above the activation energy for diffusion can be sustained for millions of years. Nearly all such examples require the scale of isotopic homogenization to be no greater than a few decimeters, while the scale of solid state diffusion might be no more than that necessary for diffusion of an ion from interiors to grain boundaries (mm-cm).

Middle Proterozoic Rocks in the Tusas and Picuris ranges of north-central New Mexico include a middle-amphibolte facies, supracrustal assemblage of aluminous schists, quartzites, and amphibolites, as well as intrusives such as the Embudo Granite (Picuris Range) and the Tres Piedras and Tusas Mountain Granite (Tusas Range). The thermal peak of metamorphism that affected these rocks has been well dated (U-Pb ages of staurolite) at 1461 +/- 13 Ma.[1]

We have collected samples of the Tres Piedras and Tusas Mountain granites at three localities as part of a geochronological study. U-Pb dates on zircons extracted from the Tres Piedras and Tusas Mountain granites indicate a crystallization age of these rocks of 1654+/- 17 Ma. Rb- Sr whole-rock isochrons yielding ages and initial $^{87}Sr/^{86}Sr$ ratios of 1463 +/- 21 Ma (0.7183 +/- 0.0006), 1471 +/- 34 Ma (0.7145 +/- 0.0008, and 1455 +/- 20 Ma (0.7102 +/- 0.0008) have been obtained from rocks from the three separate localities.

These data point to an extraordinary scale of strontium isotopic homogenization in non-convecting rocks. The coincidence (within uncertainties) of the isochron ages indicate that during the regional metamorphic episode, the strontium in these rocks were isotopically homogenized over a scale of 10 to 400 meters (the range of distance between samples at a single locality). The distinctly different $^{87}Sr/^{86}Sr$ initial ratio values of the three isochrons indicate that the scale of isotopic homogenization was less than a few kilometers (the minimum distance between collecting localities).

It seems that such large scale homogenization in rocks that still retain most of their original igneous fabric must involve isotopic exchange and communication with a hydrothermal phase. Additional analyses are planned to better constrain the scale of isotopic homogenization and identify the role of water-rock interaction.

1 Lanzirotti, A. and Hanson, G.N., Contrib. Mineral. Petrol. **129,** 352-365 (1997)

## Parametrization of Trace Element Partitioning on the Mantle Solidus

Salters, V.J.M., NHMFL, Geological Sciences
Longhi, J., Columbia Univ., Lamont-Doherty Earth Observatory

We have determined experimentally the partitioning of Y, Nb, Ce, Nd, Sm, Er, Yb, Lu, Hf, U, Th, and Pb for garnet, clinopyroxene and orthopyroxene at pressures up to 3.4 GPa. The pressures, temperatures and compositions at which we determined the partitioning is representative of the conditions near the mantle solidus. Most of the new experimental data confirm our previous studies (Salters and Longhi 1999) in terms of both absolute levels of partition coefficients for these elements as well as our first order model to explain the variations. The new data allows further assessment of the compositional and pressure and temperature dependence of the partition coefficients (Ds) and parametrization of the Ds up to 3.4 GPa, although the cause and effect of indiidual parameters are still hard to distinguish. Our highest pressure data shows that the absolute Ds for the heavy REE at higher pressures decreases; $D_{Lu}$ for garnet varies between 4 and 6 at 3.4 GPa, while $D_{Lu}$ reaches values up to 12 at 2.8 GPa. $D_{REE}$ for garnet seems to correlate best with melt structure, measured as non-

bridging oxygens (NBO) over tetrahedral silica (T). The Ds are highest in garnets in equilibrium with the most polymerized melt (lowest NBO/T).

Enough partitioning data is now available to allow a systematic description of the variations of the partition coefficients as a function of pressure, temperature and composition. There are two different ways partitioning behavior can be parametrized:

- Using theory that describes how well the substituting ion "fits" in the crystal lattice (Wood and Blundy 1997). This parametrization describes the crystal chemical controls partitioning as a function of the size of the substituting ion, the optimum size of the site and the rigidity of the crystal lattice.
- Using thermodynamic descriptions for exchange reactions or formation reactions out of melt components. This approach yields information on the enthalpy and entropy a of reaction. In addition first order Margules parameters are used to describe the excess free energy of mixing. This approach is very similar to the one used by Gaetani and Grove (1995)

We found that for both garnet and clinopyroxene best descriptions of the partitioning behavior are made using the thermodynamic descriptions. Multiple lineair regressions using the minimum number of variables produce fits with $R^2$ values consistently larger than 0.8. Best descriptions of partitioning behavior are found if the melts is parametrized according to Bottinga and Weill (1972). Although these parametrizations are able to model the partition behavior accurately within the composition range of the experiments the thermodynamic constants calculated from these regressions are not always realistic. Partitioning experiments over a wider range of compositions would yield more realistic thermodynamic constants but would not necessarily lead to more accurate predictions of partition coefficients.

Parametrization describing crystal chemical controls as described by Wood and Blundy yields to correlation between observed and predicted partition coefficents with $R^2$ of less than 0.5. This correlation can be improved significantly if a parametrization is also a function of the melt structure (described as either number of non-bridging oxygens over tetrahedral silicas or as alkalinity of the melt), but this parametrization is still less accurate then the pure thermodynamic approach.

Enough partitioning information is now available to allow assessment of partitioning behavior during melting of garnet peridotite as well as garnet pyroxenite and it can be shown that melts from these two different lithologies have distinctive U-Th, Sm-Nd and Lu-Hf isotope and trace element systematics (Stracke *et al*, 1999). Compared to melts from a garnet-pyroxenite or eclogite, melts from a garnet-peridotite are significantly more enriched in Th compared to U, leading to larger Th-excesses in garnet-peridotite derived melts. Compared to garnet-pyroxenite or eclogite, Lu-Hf fractionation is smaller, and Sm-Nd fractionation is larger during melting of garnet-peridotite. Thus, for similar degrees of melting, garnet-peridotite derived melts have significantly larger Th-excesses, and lower Lu/Hf and Sm/Nd ratios compared to garnet-pyroxenite derived melts. It can be shown that the isotope and trace element variations at Hawaii are incompatible with the presence of garnet pyroxenite in the source of Hawaiian basalts (Stracke *et al*, 1999).

1 Bottinga and Weill, Am. J. Sci. **272**, 438-475 (1972).
2 Gaetani and Grove, Geochim. Cosmochim. Acta **59**, 1951-1962 (1995).
3 Salters and Longhi, Earth Plan. Sci. Lett., **166**, 15-30 (1999)
4 Stracke *et al,* G3, 1st Issue, (1999).
5 Wood and Blundy, Contrib.Mineral. Petrol. **129**, 166-181( 1997).

## Rare-Earth-Element and Trace-Element Trends in the Everglades as Tracers for Sedimentary Processes

Sonke, J.E., NHMFL, Geological Sciences
Salters, V.J.M., NHMFL, Geological Sciences

Ecological changes in the Everglades resulting from eutrophication have been suggested to be directly related to the application of fertilizers in the Everglades Agricultural Area (EAA)[1,2]. We measured Rare Earth Elements (REE) and trace elements in surface waters, plants, peat sediments, fertilizers and bed-rock from EAA, Environmental Nutrient Removal area (ENR) and Water Conservation Area (WCA), covering a range of human influenced to pristine wetland ecosystems. Results show decreasing P concentrations in sediments and waters towards pristine Everglades (Figure 1; F1 toward U3), and decreasing P concentrations with depth. U concentrations in waters and sediments strongly correlate with P (Figure 1) and can be explained by an enrichment of U in fertilizer[3].

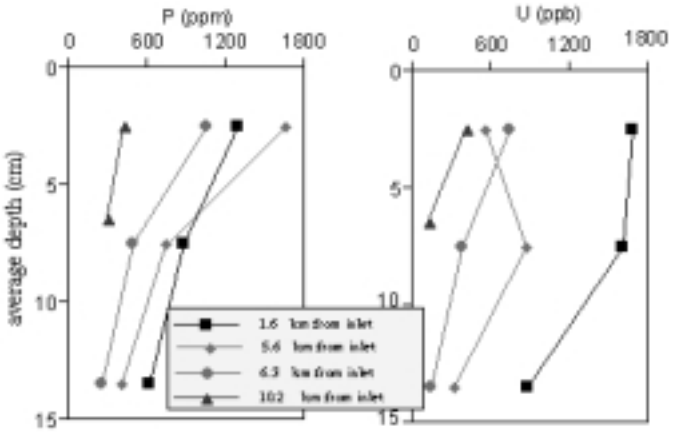


**Figure 1.** Down-core P and U concentrations at increasing distances from the Hillsborough canal inlet in WCA 2A. A decrease with depth and distance for both P and U is observable, and can be related to agricultural runoff into the WCA's.

A survey of REE trends in samples from WCA 2A and fertilizers is shown in Figure 2. Fertilizers applied in the EAA show distinct Light REE depleted patterns relative to North American Shale. This is reflected in low Pr/Yb ratios of 0.78. Carbonate bedrock and clay minerals are LREE enriched with Pr/Yb ratios of 2.7 and 2.8 respectively. Sediments, on average consisting

of 86wt.% organic matter, 2wt.% clay and 12wt.% carbonate, have Pr/Yb ratios of 3.8 suggesting the organic matter source to be enriched in LREE to an even larger extent. The large LREE enrichment is indeed reflected in living plants with Pr/Yb ratios of 7.8. The ability of plants to fractionate REE (higher LREE uptake relative to HREE) has been observed by other workers and must result in a LREE depletion of its uptake source. Pr/Yb ratios of water average 0.36 and allow us to postulate an open ecosystem model in which plants fractionate LREE from waters, thereby enriching peat sediments and depleting the water source in LREE. REE mass balance calculations on the three major fractions of the sediments, organic, carbonate and clay allow a quantification of O.M. recycling. An exponential decrease in organic matter breakdown was found, with a recycling efficiency of almost 90% in the upper 5 cm (Figure 3, ages estimated by sedimentation rates of [2]). The decreasing P and U concentrations with depth (Figure 1), therefore result from both anthropogenic inputs from agricultural runoff as well as biological recycling.

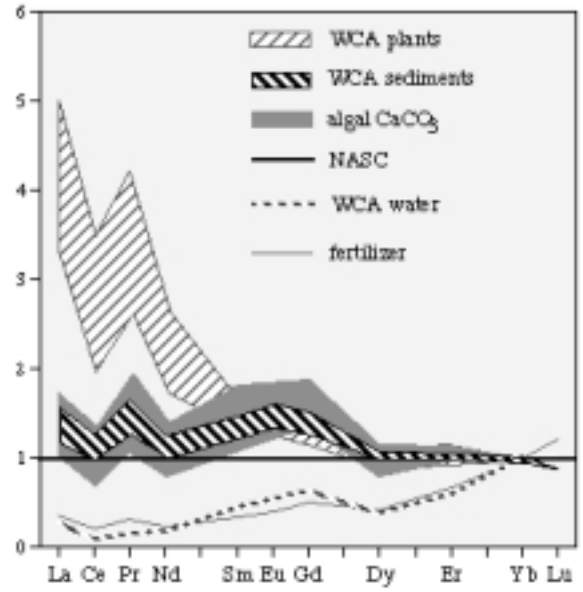


**Figure 2.** Yb-normalized (chondrite-normalized) REE patterns for WCA 2A samples.

This study illustrates the usefulness of trace elements in quantifying surface processes and tracing anthropogenic inputs into the surface environment. Fractionation of REE by plants provides a convenient way for mass balancing soil processes, which define the basic framework for interpreting anthropogenic stressors such as P.

1 Reddy, K.R. *et al.* (1993) Soil Sci. Soc. Am. J., **57**, 1147-1155.
2 Craft, C.B. and Richardson, C.J. (1998) Soil Sci. Soc. Am. J., **62**, 834-843.
3 Zielinski, R.A., *et al.* Applied Geochemistry, **15**, 369-383, (2000).

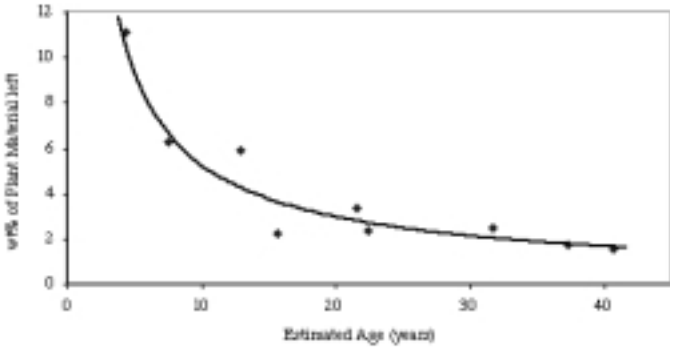


**Figure 3.** Weight percentage of organic matter left as a function of sediment age. Ages were estimated from sedimentation rates of Ref.[3] for locations along the nutrient gradient. 90% of the O.M. is recycled in the first 5 years, followed by an exponential decrease.

## Distribution and Carbon Isotopic Composition of Dissolved Organic Matter in Florida Everglades

Wang, Y., NHMFL/FSU, Geological Sciences
Hsieh, Y.P., FAMU, Wetland Ecology Program
Landing, W.M., FSU, Oceanography
Choi, Y., NHMFL/FSU, Geological Sciences
Salters, V.J.M., NHMFL/FSU, Geological Sciences
Cooper, W., NHMFL/FSU, Chemistry
Proctor, L., NHMFL/FSU, Oceanography

The distribution and natural carbon isotopic ratios of dissolved organic matter (DOC) reflect the sources and fates of DOC in an ecosystem. In the surface waters in the Florida Everglades area, DOC can come from the historic peat deposits, "modern" wetland vegetation and sugarcane (the dominant agricultural crop in the Everglades Agricultural Area). $\delta^{13}C$ analyses of DOC, plants and soils collected from the Everglades area indicate that less than 22% of the DOC was derived from sugarcane and the amount of DOC from sugarcane was greater in the dry season than in the wet season. Radiocarbon ages of DOC ranged from "modern" to about 2000 years BP, indicating that DOC was derived from both old peat deposits and modern wetland vegetation. The high molecular weight DOC (>1000 Dalton) had older radiocarbon ages than the low molecular weight DOC (<1000 Dalton), and contained a greater fraction of DOC derived from the old peat deposits. It appears that at least some of the old DOC derived from historic peat deposits was decomposed by microbes during their residence in the canal and in the Water Conservation Area, and the low molecular weight DOC was more microbially labile than the high molecular DOC.

## Radiocarbon Isotopic Variations in Soil $CO_2$ Flux

Wang, Y., NHMFL/FSU, Geological Sciences
Amundson, R., Univ. of California at Berkeley, Division of Ecosystem Science
Niu, X-F., FSU, Statistics

It has been widely accepted that an increase in temperature would accelerate microbial decomposition of soil organic matter, which would provide a positive feedback to global warming. Soil moisture, however has received little attention in C cycle studies. In this study, we developed a technique for sampling soil respired $CO_2$ for isotopic measurements and a model that relates the radiocarbon content of soil respired $CO_2$ to the rate of C cycling in soils. We measured soil $CO_2$ flux, carbon isotopic content of soil respired $CO_2$, soil temperature and soil moisture on a monthly basis along an elevation transect in the Sierra Nevada. Both soil $CO_2$ flux and its radiocarbon content displayed significant variations, spatially and temporally, in response to changes in soil temperature and moisture. The apparent decay rate of soil organic matter derived from the radiocarbon content of soil respired $CO_2$ increased with increasing temperature when soil moisture was adequate, but decreased with increasing temperature when soil moisture became limited. The apparent decay rate of soil organic matter also varied with soil moisture. Higher soil moisture content accelerated decomposition of soil organic matter until it reached an optimal level, and then inhibited decomposition when more pores in soils became saturated with water and perhaps oxygen availability (for microbes) became limited. Although the rate of soil organic matter decomposition varied throughout the year in response to fluctuations in soil temperature and moisture, the maximum apparent decay rate was higher at the low elevation site than at the high elevation sites. Litter decomposition simulated by measuring changes in mass of litter in litter bags placed in the field also showed similar decomposition pattern with decreasing decomposition rate with elevation. Multi-variable regression analyses suggest that soil moisture was a major factor controlling the rate of soil organic matter decomposition and soil $CO_2$ flux in the Sierra Nevada soils. It appears that both decomposition and total soil $CO_2$ flux are related significantly to soil moisture, temperature, and site effects.

## Major, Trace Element, and Nd-Sr-Pb Isotope Studies of Cenozoic Basalts in SE China: Mantle Sources, Regional Variations, and Tectonic Significance

Zou, H., Univ. of California at Los Angeles, Earth and Space
Zindler, A., NHMFL/FSU, Geological Sciences

Major and trace elements and Nd, Sr, and Pb isotopic compositions of xenolith bearing Cenozoic basalts in southeastern China provide important insights into the nature of mantle character and processes in this region. These basalts are LREE-enriched, and have positive Nb and Ta anomalies, and negative Pb anomalies. Although they have Sr and Nd isotope ratios similar to Hawaiian basalts, their elevated $^{207}Pb/^{204}Pb$ and $^{208}Pb/^{204}Pb$ resemble those of southern hemisphere DUPAL oceanic islands. The negative relationship between $^{143}Nd/^{144}Nd$ and $^{206}Pb/^{204}Pb$, and the positive relationship between $^{87}Sr/^{86}Sr$ and $^{206}Pb/^{204}Pb$, strongly suggests a mixing between intermediate-depleted asthenospheric mantle and an EM2 component in the mantle beneath SE China. The occurrence of the EM2 signature, and its northward decrease, is consistent with the hypothesis that SE China was once a part of the supercontinent Gondwanaland.

When isotopic data from NE China are included, $^{206}Pb/^{204}Pb$ is seen to decrease from south to north through the whole of eastern China. However, the regional variation of Pb isotopic compositions cannot simply be attributed to the mixing of two mantle source components throughout this region because Sr and Nd isotopic variations are distinctly different in the north and south. In SE China, $^{143}Nd/^{144}Nd$ increases and $^{87}Sr/^{86}Sr$ decreases to the north, while the opposite is true in NE China. Thus, while SE China basalts suggest a mixing between depleted asthenospheric mantle and EM2, NE Chinese basalts appear to result from mixing between asthenospheric mantle and EM1. Basalts from central China (Nushan, Fagshan, and Tashan) have the highest $^{143}Nd/^{144}Nd$ and the lowest $^{87}Sr/^{86}Sr$ of all Chinese Cenozoic basalts, and may represent the isotopic composition of the asthenospheric mantle beneath China. These basalts, however, still show some DUPAL-like elevation of Pb isotopes, suggesting that the asthenospheric mantle has this character prior to the further mixing suggested for the eastern Chinese basalts.

## Theoretical Studies of $^{238}U$-$^{230}Th$-$^{226}Ra$ and $^{235}U$-$^{231}Pa$ Disequilibria in Young Lavas Produced by Mantle Melting

Zou, H., Univ. of California at Los Angeles, Earth and Space
Zindler, A., NHMFL/FSU, Geological Sciences

This work provides ready-to-use equations to express the variations of $(^{230}Th/^{238}U)$, $(^{226}Ra/^{230}Th)$, and $(^{231}Pa/^{235}U)$ as functions of melting porosity, melting rate, and melting time. Modeling results have shown that, low melting porosity, slow melting rate, and short melting time favor the generation of lavas with high values of $(^{230}Th/^{238}U)$, $(^{226}Ra/^{230}Th)$, and $(^{231}Pa/^{235}U)$. If melting takes place in spinel peridotite mantle, the same is true for $(^{226}Ra/^{230}Th)$, and $(^{231}Pa/^{235}U)$, but the reverse is true for $(^{230}Th/^{238}U)$. $(^{226}Ra/^{230}Th)$ is very sensitive to melting porosity, with significant $^{226}Ra$ excesses indicating small porosity.

This work also clearly defines melting rate in the context of the dynamic melting model. In addition, the uranium decay

series (U-series) modeling is quantitatively compared with trace element modeling. Trace element fractionation depends on how much of the source is melted, whereas U-series disequilibria is dependent not only on how much of the source is melted but also on how rapidly it is melted. Both net elemental parent-daughter (e.g., U-Th) fractionation and the daughter (e.g., $^{230}$Th) ingrowth contribute to the total U-series disequilibria. The relative contribution from net elemental fractionation and that from daughter ingrowth to total U-series disequilibria are further quantified. The daughter ingrowth is generally important in the generation of U-series disequilibria, particularly when the daughter has a short half-life (e.g., $^{226}$Ra) and the melting rate is slow. Therefore, U-series disequilibria can not be attributed to net elemental fractionation alone. Some previous approaches to modeling U-series disequilibria using the equations for trace element fractionation are not sound in principle. Such approaches ignore the significant contribution from daughter ingrowth and would incorrectly require extremely small degrees of melting to explain the U-series disequilibria in young lavas.

# SUPERCONDUCTIVITY – BASIC

## "Magnetic" Ground State in Multiband Superconductors

Agterberg, D.F., NHMFL
Barzykin, V., NHMFL
Gor'kov, L.P., NHMFL

The pairing states due to the usual BCS mechanisms are considered[1,2] in substances of cubic and hexagonal symmetry where the Fermi surfaces form pockets around several points of high symmetry. It turns out that the symmetry imposed on the multiple pocket positions could give rise to a multidimensional nontrivial superconducting order parameter. If so, the time-reversal symmetry in the pairing state is broken. While all these non s-wave states are destroyed by non-magnetic impurities, the suppression is much weaker than would be expected for unconventional superconductors with isotropic non-magnetic impurity scattering. Several candidate substances where such ordering may appear. The list includes such materials as $CeCo_2$, $CeRu_2$, and $LaB_6$, all of which have the proper Fermi surface topology. In addition to the phase-sensitive experiments, nontrivial character of the order parameter may be observed by more traditional experiments provided that a Fermi surface pocket embraces the Zone center.

[1] Agterberg, D.F., *et al*., Europhys. Lett., **48**, 449 (1999).
[2] Agterberg, D.F., *et al.,* Phys. Rev. B, **60**, 14868 (1999).

## Unconventional Cyclotron Resonance Observed in $Sr_2RuO_4$

Ardavan, A., Univ. of Oxford, Physics
Edwards, R., Univ. of Oxford, Physics
Rzepniewski, E., Univ. of Oxford, Physics
Schrama, J.M., Univ. of Oxford, Physics
Singleton, J., Univ. of Oxford, Physics
Maeno, Y., Kyoto Univ., Japan

The layered perovskite oxide superconductor $Sr_2RuO_4$ was discovered in 1994.[1] Since then it has generated much interest, both theoretical and experimental, including measurements of magnetic quantum oscillations, the effect of non-magnetic impurities, heat capacity, Knight shift, and muon spin rotation; evidence for a ferromagnetically-mediated spin-triplet p-wave groundstate seems strong.[2,3,4] Evidence for strong electron correlations has stimulated interest in measuring cyclotron resonance,[3] since it has been proposed that the contributions to the effective mass renormalization from electron-electron interactions and electron-phonon interactions can be separated by comparing the mass measured by cyclotron resonance with the effective mass found in thermodynamic measurements and the calculated band mass.[5] Recently, a measurement of cyclotron resonance in $Sr_2RuO_4$ has been reported.[3] In that study, however, there was no measurement of the dependence of the observed resonances on magnetic field orientation; measurement of the angle-dependence has been shown to be important in other low-dimensional systems.[6]

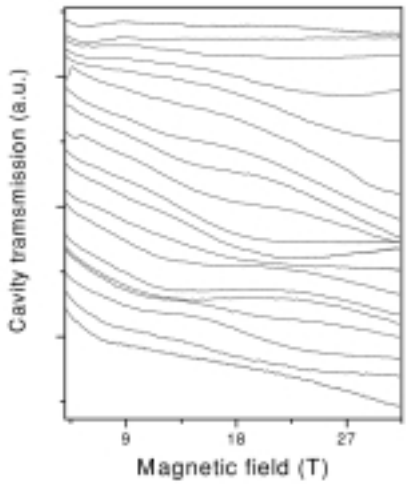


**Figure 1.** Millimeter-wave response of $Sr_2RuO_4$ at 70 GHz and 0.6 K; the amplitude transmission of a resonant cavity containing the sample is shown; a minimum corresponds to a resonance in the high-frequency conductivity of the sample. The angle range is 0 degrees (top trace) to 70 degrees (bottom trace). Several resonances are visible, exhibiting strongly angle-dependent behavior.

Using the 33 T steady fields at NHMFL, we measured the angle dependence of the millimeter-wave response of $Sr_2RuO_4$ at 70 GHz and 0.6 K. Figure 1 shows the raw data obtained (the amplitude transmission of a resonant cavity containing the sample is shown; a minimum corresponds to a resonance in the high-frequency conductivity of the sample). The angle range